Journal of Power Sources 307 (2016) 684–689

Contents lists available at ScienceDirect

Journal of Power Sources

journal homepage: www.elsevier.com/locate/jpowsour

Short communication

Radio frequency magnetron sputtering of $Li_7La_3Zr_2O_{12}$ thin films for solid-state batteries

S. Lobe [a, b, *], C. Dellen [a, b], M. Finsterbusch [a, b], H.-G. Gehrke [a, b], D. Sebold [a, b], C.-L. Tsai [a, b], S. Uhlenbruck [a, b], O. Guillon [a, b, c]

[a] Forschungszentrum Jülich GmbH, Institute of Energy and Climate Research (IEK-1), Materials Synthesis and Processing, 52425 Jülich, Germany
[b] Jülich Aachen Research Alliance: JARA Energy, Germany
[c] Rheinisch-Westfälische Technische Hochschule (RWTH) Aachen, Institut für Gesteinshüttenkunde, Mauerstr. 5, 52064 Aachen, Germany

HIGHLIGHTS

- Thin films of cubic $Li_7La_3Zr_2O_{12}$ are deposited by r.f. magnetron sputter deposition.
- Substrate temperatures of 700 °C and higher are required for single phase thin films.
- Oxidation layer is formed on substrate surface at 700 °C and higher.
- Li-ion conductivity is 1.2×10^{-4} S cm^{-1} with an activation energy of 0.47 eV.

ARTICLE INFO

Article history:
Received 13 November 2015
Received in revised form
9 December 2015
Accepted 16 December 2015
Available online xxx

Keywords:
Thin film
$Li_7La_3Zr_2O_{12}$
Magnetron sputter deposition
Solid electrolyte
Solid-state batteries

ABSTRACT

Thin film batteries based on solid electrolytes having a garnet-structure like $Li_7La_3Zr_2O_{12}$ (LLZ) are considered as one option for safer batteries with increased power density. In this work we show the deposition of Ta- and Al-substituted LLZ thin films on stainless steel substrates by r.f. magnetron sputtering. The thin films were characterized by XRD, SEM and time-of-flight-secondary ion mass spectrometry (ToF-SIMS) to determine crystal structure, morphology and element distribution. The substrate temperature was identified to be one important parameter for the formation of cubic garnet-structured LLZ thin films. LLZ formation starts at around 650 °C. Single phase cubic thin films were obtained at substrate temperatures of 700 °C and higher. At these temperatures an interlayer is formed. Combination of SEM, ToF-SIMS and XRD indicated that this layer consists of γ-$LiAlO_2$. The combined total ionic conductivity of the γ-$LiAlO_2$ interlayer and the LLZ thin film (perpendicular to the plane) was determined to be 2.0×10^{-9} S cm^{-1} for the sample deposited at 700 °C. In-plane measurements showed a room temperature conductivity of 1.2×10^{-4} S cm^{-1} with an activation energy of 0.47 eV for the LLZ thin film.
© 2016 Elsevier B.V. All rights reserved.

1. Introduction

Solid electrolytes are considered to play an important role for the development of high performance batteries for future applications in *e.g.* electric vehicles, stationary energy storage and portable electronics. Besides the advantage of building an inherently safer battery by replacing the liquid electrolyte in conventional Li-ion batteries, solid electrolytes can also be used as separators in Li–O_2 and Li–S cells. Some sulfide [1], oxide [2] and phosphate [3] materials show a high Li-ion conductivity which makes them suitable as solid electrolytes. Promising oxides are garnets based on $Li_7La_3Zr_2O_{12}$ (LLZ) [4]. Substitution of Li or Zr in LLZ leads to a stabilization of the cubic garnet structure at room temperature and an increase in Li-ion conductivity. Common substituents are Ta [5], Al [6] and Nb [7]. LLZ has a reasonable Li-ion conductivity (up to 9.6×10^{-4} S cm^{-1} [5]) and shows also remarkable chemical (*e.g.* against Lithium [8]), electrochemical (up to 8 V [6]) and thermal stability (up to 1000 °C) which offers a wide range of applications, especially for high voltage Li-ion batteries. Solid state batteries composed of a $LiCoO_2$ cathode, a garnet-structured electrolyte and a lithium anode have already been

* Corresponding author. Forschungszentrum Jülich GmbH, Institute of Energy and Climate Research (IEK-1), Materials Synthesis and Processing, 52425 Jülich, Germany.
E-mail address: s.lobe@fz-juelich.de (S. Lobe).

http://dx.doi.org/10.1016/j.jpowsour.2015.12.054
0378-7753/© 2016 Elsevier B.V. All rights reserved.

demonstrated [9,10]. These cells showed a high internal resistance, probably due to the lower ionic conductivity compared to conventional liquid electrolytes. Thin film deposition of the electrolyte on anode or cathode material can reduce the resistance by 1–2 orders of magnitude. The concept of an all solid state thin film lithium battery has already been shown with a lithium phosphorous oxynitride glass electrolyte (LiPON) [11,12]. Careful adjustment of consecutive processes leads to defect reduced interfaces and thus, reduced interface resistivity. When using a $LiCoO_2$ cathode and a Li anode, an utilization of more than 80% of cathode material was achieved [13]. Several approaches for thin film deposition of LLZ by sol–gel [14,15], pulsed laser deposition (PLD) [16–18], metal organic chemical vapor deposition [19], aerosol deposition [20] and radio-frequency (r.f.) magnetron sputtering [21,22] were reported in literature. Common problems during deposition are the amorphous structure of the LLZ films when deposited at room temperature and the Li-loss resulting in $La_2Zr_2O_7$ formation during crystallization at high temperature. One approach is the introduction of extra Li to compensate the loss of Li, which is often used for PLD and sol–gel processes [14,15,17,18]. Avoiding the formation of $La_2Zr_2O_7$ can be achieved by depositing Zr-free garnets $Li_6BaLa_2Ta_2O_{12}$ [17] and $Li_5La_3Ta_2O_{12}$ [22]. Lattice matching materials like $Gd_3Ga_5O_{12}$ [16] can also help to crystallize the cubic structure. For our investigations, r.f. magnetron sputtering is used due to its scalability from laboratory up to industrial scale. Sputter deposition processes for different cell components like cathodes (*e.g.* $LiCoO_2$ [23], $LiFePO_4$ [24], $LiMn_2O_4$ [25]), electrolytes (*e.g.* LiPON [26], $Li_{1+x}Al_xTi_{2-x}(PO_4)_3$ (LATP) [27]) and anodes (*e.g.* $Li_4Ti_5O_{12}$ [28], $LiNiVO_4$ [29]) can be found in literature. The fabrication of amorphous Li–La–Zr–O thin films by r.f. magnetron sputter deposition was reported by Kalita et al. [21]. However, the deposition of crystalline garnet-structured LLZ thin films with a reasonable Li-ion conductivity was not reported yet.

In this work we give a detailed report about the influence of the substrate temperature on the formation of LLZ in thin films by r.f. magnetron sputtering on Aluchrom YHf (EN 1.4767) substrate and their resulting properties.

2. Experimental

2.1. Target preparation

As target material $Li_{6.6}La_3Zr_{1.6}Ta_{0.4}O_{12}$ was chosen due to its higher Li-ion conductivity and easier stabilization of the cubic phase compared to $Li_7La_3Zr_2O_{12}$. LLZ powder was prepared by solid state reaction. $LiOH\times H_2O$ (Merck, 98%), La_2O_3 (Merck, 99.9%), ZrO_2 (Treibacher, 99.5%) and Ta_2O_5 (Inframat, 99.95%) were mixed stoichiometric with a Li-excess of 15 mol-%. Pressing of the milled powder into pellets and calcination at 850 °C for 20 h were done at a first step. A repetition of milling and pressing steps was also carried out before a second and third calcination step at 1000 °C. The exact composition of the powder after all calcination steps was determined by inductive-coupled plasma optical emission spectroscopy (ICP-OES, ThermoScientific iCAP 6300) to be $Li_{7.9}Al_{0.2}La_3Zr_{1.6}Ta_{0.4}O_{12.9}$. A small amount of Al uptake from the used Al_2O_3 crucibles was observed. X-ray diffraction revealed the cubic garnet structure of the as-prepared powder. The target was prepared by pressing the powder on a Cu-backing plate.

2.2. Thin film deposition

Thin film depositions were carried out in a cluster PVD system manufactured by VonArdenne. LLZ thin films were deposited via r.f. magnetron sputtering in a pure Ar-plasma at 5×10^{-3} mbar. The sputter power was 1.2 W cm^{-2} and a bias power of 0.1 W cm^{-2} was applied. Aluchrom YHf (EN 1.4767) foil purchased by VDM metals was used as substrate for all depositions. The substrates were cleaned with acetone and 1-propanol. Residual contaminations were eliminated by Ar sputter etching before deposition. In order to determine LLZ crystallization temperature, depositions were done at substrate temperatures from 150 °C up to 800 °C. Except the sample deposited at 150 °C, all samples were heated with a closed shutter and a ramp rate of 7 K min^{-1} before deposition. The deposition was followed by a cooling to room temperature with a closed shutter and a ramp rate of 3 K min^{-1}.

2.3. Material characterization

XRD was carried out with a Bruker D4 Endeavour (Bruker AXS, Germany) using Cu-K_α radiation. SEM was conducted by using a Zeiss Ultra 55 SEM (Carl Zeiss NTS GmbH, Germany). The depth profile of element distribution was determined by using Time-of-flight secondary ion mass spectrometry (ToF-SIMS). ToF-SIMS measurements were carried out with a ToF-SIMS IV instrument (IONTOF GmbH, Germany). Cs^+ was used as sputter ion with ion beam energy of 2 keV. The sputtered area was 300 μm × 300 μm. For analysis Bi_3^+ ions with ion beam energy of 25 keV were used. The analyzed area was 80 μm × 80 μm. Impedance spectroscopy data was collected by using a Solartron Modulab 2100A multipotentiostat. The used frequency range was 1 MHz–0.1 Hz. On top of the samples four gold contacts were deposited by direct current (d.c.) magnetron sputtering. The contacts had an area of 1 mm × 7 mm and a distance of 0.5 mm to each other. Two different set-ups were used for measuring impedance data a) perpendicular to the thin film b) parallel to the thin film. All electrochemical tests were carried out in an Ar glovebox. Inert atmosphere was not broken between deposition and measurement.

3. Results

3.1. Composition and microstructure

The X-ray diffraction patterns for the samples deposited at 150 °C, 600 °C, 650 °C, 700 °C and 800 °C are shown in Fig. 1. Significant differences are observed in the diffraction patterns of the samples deposited between 150 °C and 700 °C. The diffraction pattern of the thin film deposited at 150 °C exhibits an amorphous bump around $2\theta = 29°$ and a reflection at $2\theta = 44.5°$ which can be attributed to the used substrate. At 600 °C several reflections indicate the crystalline behavior of the thin film. $La_2Zr_2O_7$ can be identified as main phase and only small amounts of garnet-structured phase can be observed. The remaining small reflections (marked with *) fit to the structure of $La_{24}Ce_{12}Li_{24}O_{72}$ [30]. A contamination of the samples with Ce was excluded by ICP-MS (Agilent 7500ce). The occupation of the different sites in the structure is not obvious from the measurement. The diffraction pattern of the deposition at 650 °C exhibits an increasing fraction of the cubic LLZ phase. Nevertheless, a large amount of $La_2Zr_2O_7$ is still observed. This thin film still shows reflections of a phase similar to $La_{24}Ce_{12}Li_{24}O_{72}$. In case of the deposition with a substrate temperature of 700 °C the diffraction pattern shows only single phase garnet-structured LLZ and the substrate reflection. At deposition temperatures of 800 °C, the diffraction pattern reveals cubic LLZ as main phase and the substrate reflections, too. However, additional reflections of secondary phases are visible. These reflections fit to several patterns of binary and ternary oxides consisting of Li, Al, Fe and Cr. For example, the reflections marked with "+" fit well to the diffraction pattern of γ-$LiAlO_2$ (PCPDF# 01-073-1338). A final conclusion about the origin of these additional reflections cannot be drawn because the identification of phases by one or two

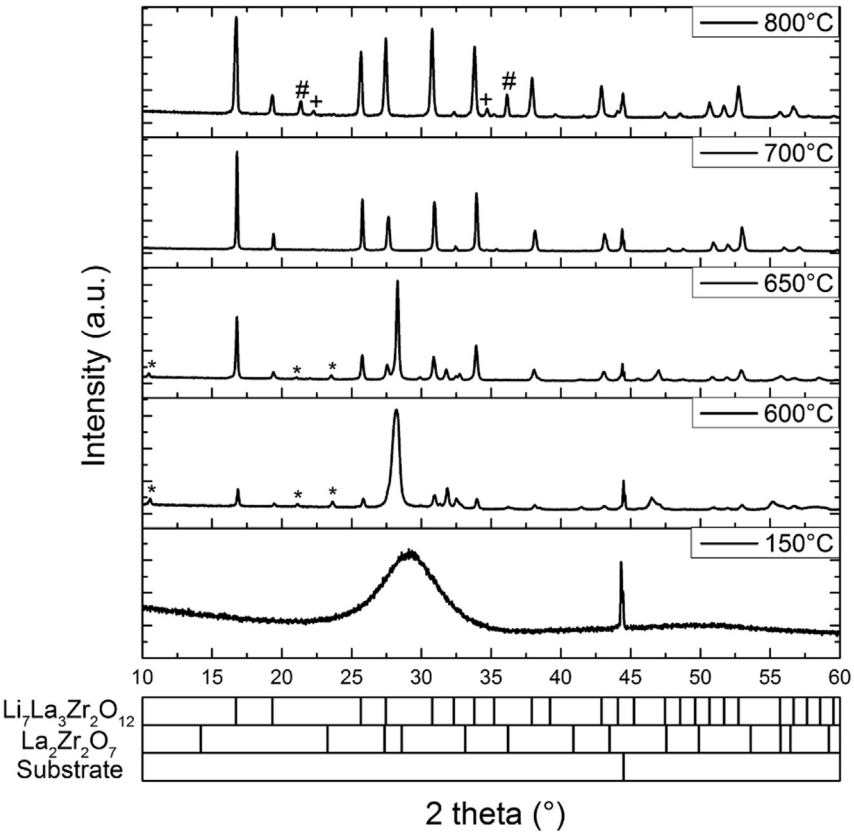

Fig. 1. X-ray diffraction patterns of thin films sputtered at different substrate temperatures. * = $La_{24}Ce_{12}Li_{24}O_{72}$+ = γ-$LiAlO_2$ # = unknown phase.

reflections is not reliable. However, we expect that these reflections occur due to oxidation of the substrate either during heating or deposition. Neither at 700 °C nor at 800 °C is a preferential orientation of the garnet-structured phase visible.

The microstructure of the samples, deposited at 700 °C and 800 °C, are shown in Fig. 2. The surface of the film deposited at 700 °C shows a homogenous surface with only a small amount of defects, probably due to the rough substrate surface. The backscattered electron (BSE) image reveals no secondary phases in accordance with the XRD pattern (Fig. 2a). Closer inspection shows a dense surface (Fig. 2b). The cross-section reveals a LLZ layer thickness of around 1.8 μm and an interlayer between substrate and LLZ thin film with a thickness of around 0.2 μm. The BSE-image shows a slight porosity of the LLZ thin film. Corresponding to a low average atomic number, the darker appearance of the interlayer leads to the conclusion that it mainly consists of light elements (Fig. 2c). The surface of the sample deposited at 800 °C is covered by a lot of particle-like agglomerates (Fig. 2d). Closer inspection confirms a chemical homogenous but porous surface. The agglomerates consist of plate-like particles and exhibit a higher porosity. The plates are arranged perpendicular to the surface (Fig. 2e). The cross section of the sample shows a LLZ thin film with a thickness of around 1.8 μm. The grains have a columnar shape with large pores between the single grains. Furthermore an interlayer with a thickness of around 1 μm is visible between the thin film and the substrate (Fig. 2f). Comparison of the cross-sections of the samples deposited at 700 °C and 800 °C indicates an increasing substrate roughness due to surface oxidation.

3.2. Element distribution

The element distributions of the thin films were examined in order to get more detailed information about the element contents of the certain layers. ToF-SIMS depth profiles were measured until the Aluchrom YHf substrate was reached, which is indicated by constant signals of $CsFe^+$ and Cr^+. The depth profiles for the samples deposited at 150 °C, 700 °C and 800 °C are shown in Fig. 3. In general, the signals of LaO^+ and ZrO^+ are nearly identical for all temperatures. The minimum of both signals followed by a maximum between 2000 s and 3000 s for the sample deposited at 800 °C can be explained by the increasing porosity of the layer followed by a denser part close to the interlayer. The depth profile of the ZrO^+ signal reveals an overlap with the $CsFe^+$ and the Cr^+ signal at significant intensities for samples deposited at 150 °C and 700 °C, at 800 °C the signal overlap is close to the background signal, indicating a comparatively lower Zr content of the interlayer. The Li^+ intensity is increasing with increasing substrate temperature. For the sample deposited at 150 °C no $LiAlO^+$ signal can be observed, the signal has an increasing intensity with increasing substrate temperature. For the samples deposited at 700 °C and 800 °C the Al^+ signal shows the same characteristic like the $LiAlO^+$ signal. The depth profiles of the samples deposited at 700 °C and 800 °C show a broadening of the Cr^+ and the $CsFe^+$ signal, most likely due to the roughening of the surface.

3.3. Li-ion conductivity

Impedance spectra of the sample deposited at 700 °C are shown in Fig. 4. For these measurements blocking electrodes *i.e.* gold contacts and Aluchrom YHf substrate were used. The cross-section

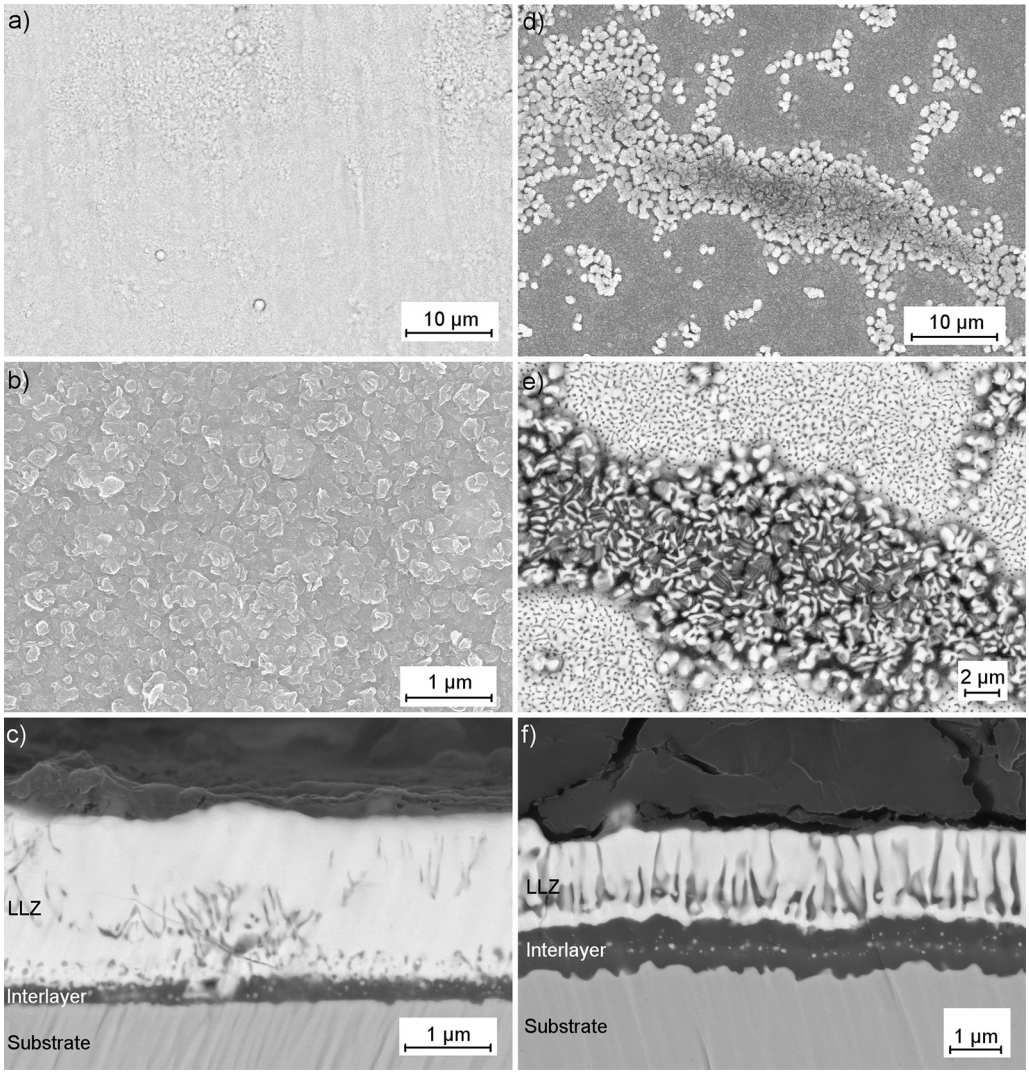

Fig. 2. Microstructure of the thin films deposited at 700 °C and 800 °C a) BSE-image, 700°C b) SE-image, 700°C c) cross-section, BSE-image, 700°C, d) SE-image, 800°C e)BSE-image, 800°C f) cross-section, BSE-image, 800°C

measurements show the beginning of a semicircle at high frequency range ending in a tail at low frequencies which indicates the blocking effect of the used blocking electrodes (Fig. 4a). From the single semicircle, the total conductivity was determined to be 2×10^{-9} S cm^{-1}. This value is very low compared to LLZ bulk-material (*e.g.* 4.7×10^{-4} S cm^{-1} for $Li_{6.6}La_3Zr_{1.6}Ta_{0.4}O_{12}$ [5]) or other LLZ thin films processed by PLD (*e.g.* $1.0 \times 10^{-5} - 2.5 \times 10^{-6}$ S cm^{-1} [16]).

In-plane measurements were also carried out between different contacts on the surface of the thin film (Fig. 4b). The resulting Nyquist diagrams reveal the beginning of a semicircle followed by a plateau and a tail. The spectra were fitted by the model circuit which is shown in the inset in Fig. 4b. While carrying out the fitting, a capacitance of 6×10^{-8} F was obtained for R1/CPE1 and 7×10^{-9} F for R2/CPE2. Since the capacitances were similar, a proper assignment of bulk and grain boundary contribution was not possible. On the other hand, when using a model circuit with three semicircles for fitting the whole spectra, all CPEs have similar capacitance at 10^{-9} range which cannot be interpreted easily by only temperature dependent measurement of the thin film. Therefore, model circuit with two semicircles was used for fitting all impedance spectra without separating the contributions. The total resistance of R1+R2 was used for calculating the total conductivity of measured thin film.

Room temperature impedance measurement gives a total in-plane conductivity of 1.2×10^{-4} S cm^{-1}. This value is similar to conductivities which were obtained for bulk-material and one order of magnitude higher than the highest value which was reported for garnet-structured thin films yet (1×10^{-5} S cm^{-1} [16]). In-plane impedance measurements at different temperatures up to 89 °C give an activation energy of 0.47 eV (Fig. 4c). This value is higher than values from bulk material. Tenhaeff et al. [31] reported activations energies for Al-doped LLZ of 0.36 and 0.44 for grain and grain boundary, respectively. The higher value indicates dominating grain boundaries, reducing the total Li ion conductivity of the thin film.

4. Discussion

XRD shows that LLZ starts to form in significant amounts at substrate temperatures of 650 °C and becomes the dominating phase of the samples at deposition temperatures of 700 °C and above. Cross-section SEM images and the SIMS depth profile reveal an interlayer which consists mainly of Li, Al and O, identified by

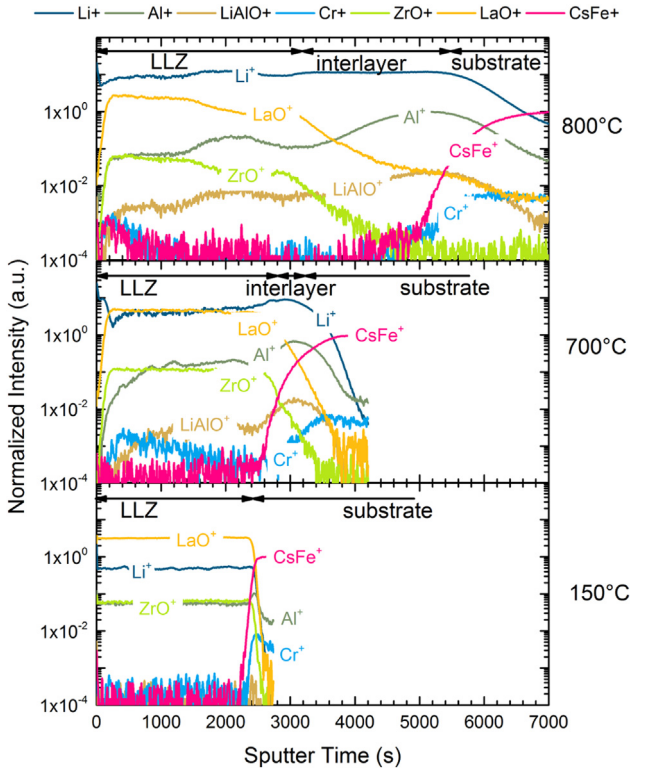

Fig. 3. ToF-SIMS depth profiles of thin films deposited at 150 °C, 700 °C and 800 °C.

XRD as γ-$LiAlO_2$. The substrate Aluchrom YHf is well known for the formation of a protective Al_2O_3 layer when heated in oxygen-containing atmospheres. Depending on the exposition time and temperature the Al_2O_3 layer consists of either a stable α-Al_2O_3 or metastable cubic aluminum oxides (γ-Al_2O_3, θ-Al_2O_3) [32]. The oxygen partial pressure during heating was around 1×10^{-8} mbar which is sufficient for the Al_2O_3 formation. The Al_2O_3 layer can react with Li during the sputtering process so that γ-$LiAlO_2$ can be formed. γ-$LiAlO_2$ is a poor electronic and Li-ion-conductor [33], which can explain the low value for cross-section conductivity obtained by impedance spectroscopy.

The SIMS depth profiles indicate an increasing Li-intensity in the thin films with increasing substrate temperature. XRD confirms the formation of Li-containing phases only at high temperatures. Both can be proof for increasing Li content with increasing substrate temperature. This is opposite to the common observation that LLZ thin films lose Li at high temperatures regarding to in-situ heating or post heat-treatment.

The increased Li content can be explained by thermodynamic phase stability. Janani et al. [34] observed a similar temperature range for the formation of cubic LLZ powder using a modified sol–gel process. However, the low Li content of the thin film deposited at 150 °C shows that the sticking coefficient of Li is very low for the used Aluchrom YHf substrate. The sticking coefficient is most likely only sufficiently high for oxide layers like Al_2O_3, so that the formation of LLZ is only allowed on such a surface layer. It is obvious that both, a combination of thermodynamics and the sticking behavior of Li on the substrate surface, influence the formation of LLZ. Further investigations have to identify substrate surface

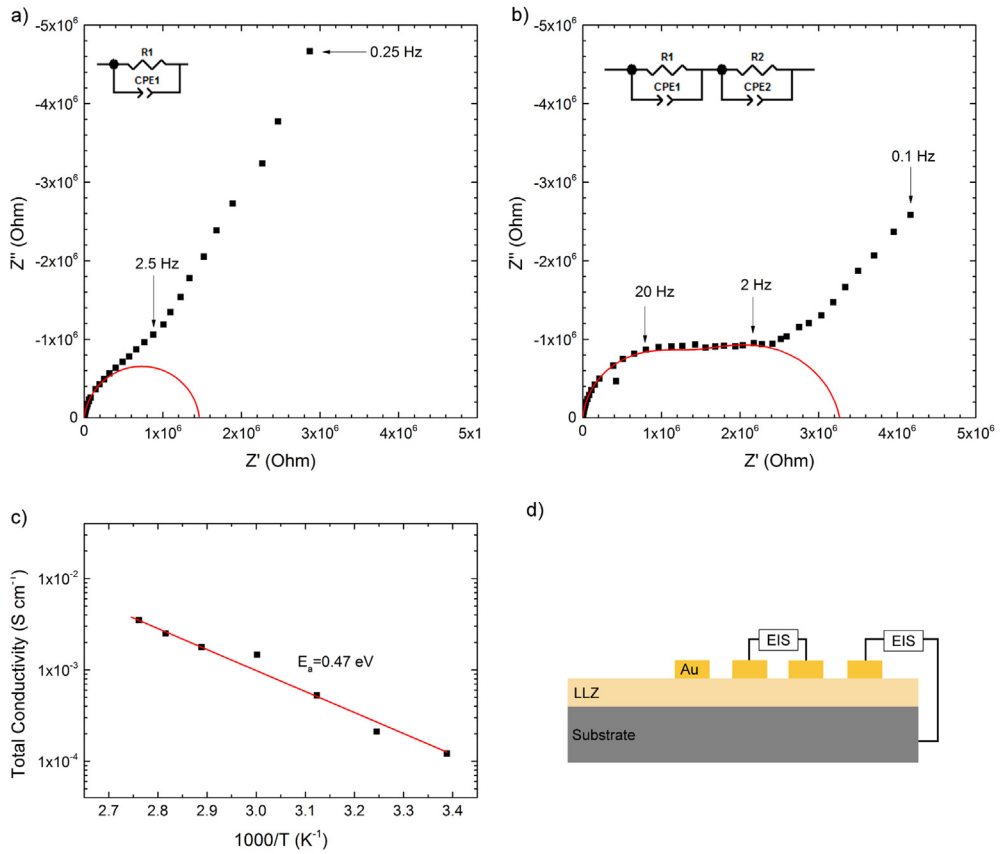

Fig. 4. Impedance data of thin film deposited at 700 °C a) Nyquist plot of the cross-section measurement b) Nyquist plot of the in-plane measurement c) Li-ion conductivity σ in dependence of temperature T d) measurement set-ups (EIS = Electrochemical Impedance Spectroscopy).

properties and related deposition conditions for cubic LLZ thin films, especially with regard to the deposition of all-solid-state thin film batteries.

5. Conclusion

Garnet-structured LLZ thin films were successfully deposited by r.f. magnetron sputtering. Deposition at different temperatures show that formation of cubic LLZ starts at deposition temperatures of around 650 °C. LLZ was the main phase with only small amount of impurities at temperatures of 700 °C and 800 °C. Closer inspection with SEM and SIMS showed that the surface of the used Aluchrom YHf substrate oxidizes resulting in an oxide interlayer at temperatures of 700 °C and higher. The thickness of the oxidation layer increases with increasing temperature. The oxidation layer, consisting of γ-$LiAlO_2$, has a high resistivity so that cross-section impedance spectroscopy showed a low ionic conductivity of only 2×10^{-9} S cm^{-1}. In-plane total Li ion conductivity was determined to be 1.2×10^{-4} S cm^{-1} at room temperature. The activation energy was determined to be 0.47 eV. The shown thin films are a promising electrolyte for solid-state Li-ion batteries.

Acknowledgment

Financial support by Helmholtz Gemeinschaft Deutscher Forschungszentren e.V. under grants “Elektrochemische Speicher im System – Zuverlässigkeit und Integration“ and “Helmholtz-Initiative für Mobile/Stationäre Energiespeichersysteme“, and by the „Bundesministerium für Bildung und Forschung“ (Federal ministry of education and research), Germany, under project no. 03X4634C (“Meet Hi-EnD”), and the Ministry of Innovation, Science and Research of North Rhine-Westphalia under project no. 424-Japan (ERA-NET) is gratefully acknowledged. We would like to thank Astrid Zimmermann (ICP-MS) and Sabrina Tückhardt (ICP-OES) from the Central Institute for Engineering, Electronics and Analytics (ZEA-3) for chemical characterization. Special thanks for the support during the depositions to Thorsten Albrecht and Frank Vondahlen.

Glossary

BSE	back scattered electrons
ICP-MS	inductive-coupled plasma mass spectrometry
ICP-OES	inductive-coupled plasma optical emission spectroscopy
LLZ	$Li_7La_3Zr_2O_{12}$ (and partially substituted relatives)
PLD	pulsed laser deposition
SE	secondary electrons
ToF-SIMS	time-of-flight secondary ion mass spectrometry

References

[1] N. Kamaya, K. Homma, Y. Yamakawa, M. Hirayama, R. Kanno, M. Yonemura, T. Kamiyama, Y. Kato, S. Hama, K. Kawamoto, A. Mitsui, Nat. Mater 10 (2011) 682–686.
[2] R. Murugan, V. Thangadurai, W. Weppner, Angew. Chem. 119 (2007) 7925–7928.
[3] Q. Ma, Q. Xu, C.-L. Tsai, F. Tietz, O. Guillon, J. Am. Ceram. Soc. (2015), http://dx.doi.org/10.1111/jace.13997.
[4] R. Murugan, V. Thangadurai, W. Weppner, Angew. Chem. Int. Ed. 46 (2007) 7778–7781.
[5] Y. Wang, W. Lai, Electrochem. Solid-State Lett. 15 (2012) A68–A71.
[6] C.-L. Tsai, E. Dashjav, E.-M. Hammer, M. Finsterbusch, F. Tietz, S. Uhlenbruck, H. Buchkremer, J. Electroceram. 35 (2015) 25–32.
[7] K. Ishiguro, Y. Nakata, M. Matsui, I. Uechi, Y. Takeda, O. Yamamoto, N. Imanishi, J. Electrochem. Soc. 160 (2013) A1690–A1693.
[8] M. Kotobuki, H. Munakata, K. Kanamura, Y. Sato, T. Yoshida, J. Electrochem. Soc. 157 (2010) A1076–A1079.
[9] M. Kotobuki, K. Kanamura, Ceram. Int. 39 (2013) 6481–6487.
[10] M. Kotobuki, K. Kanamura, Y. Sato, T. Yoshida, J. Power Sources 196 (2011) 7750–7754.
[11] B.J. Neudecker, N.J. Dudney, J.B. Bates, J. Electrochem. Soc. 147 (2000) 517–523.
[12] Y.S. Park, S.H. Lee, B.I. Lee, S.K. Joo, Electrochem. Solid State Lett. 2 (1999) 58–59.
[13] N.J. Dudney, Y.-I. Jang, J. Power Sources 119–121 (2003) 300–304.
[14] R.-J. Chen, M. Huang, W.-Z. Huang, Y. Shen, Y.-H. Lin, C.-W. Nan, J. Mater. Chem. A 2 (2014) 13277–13282.
[15] K. Tadanaga, H. Egawa, A. Hayashi, M. Tatsumisago, J. Mosa, M. Aparicio, A. Duran, J. Power Sources 273 (2015) 844–847.
[16] S. Kim, M. Hirayama, S. Taminato, R. Kanno, Dalton Trans. 42 (2013) 13112–13117.
[17] J. Reinacher, S. Berendts, J. Janek, Solid State Ion. 258 (2014) 1–7.
[18] J.J. Tan, A. Tiwari, ECS Solid State Lett. 1 (2012) Q57–Q60.
[19] H. Katsui, T. Goto, Thin Solid Films 584 (2015) 130–134.
[20] C.-W. Ahn, J.-J. Choi, J. Ryu, B.-D. Hahn, J.-W. Kim, W.-H. Yoon, J.-H. Choi, D.-S. Park, J. Electrochem. Soc. 162 (2015) A60–A63.
[21] D.J. Kalita, S.H. Lee, K.S. Lee, D.H. Ko, Y.S. Yoon, Solid State Ion. 229 (2012) 14–19.
[22] Y.N. Lee, Y.S. Yoon, Thin Solid Films 579 (2015) 75–80.
[23] J.F. Whitacre, W.C. West, E. Brandon, B.V. Ratnakumar, J. Electrochem. Soc. 148 (2001) A1078–A1084.
[24] A. Bunting, S. Uhlenbruck, C. Dellen, M. Finsterbusch, C.L. Tsai, D. Sebold, H.P. Buchkremer, R. Vassen, J. Power Sources 281 (2015) 326–333.
[25] B.-J. Hwang, C.-Y. Wang, M.-Y. Cheng, R. Santhanam, J. Phys. Chem. C 113 (2009) 11373–11380.
[26] X. Yu, J.B. Bates, G.E. Jellison, F.X. Hart, J. Electrochem. Soc. 144 (1997) 524–532.
[27] G. Tan, F. Wu, L. Li, Y. Liu, R. Chen, J. Phys. Chem. C 116 (2012) 3817–3826.
[28] C.L. Wang, Y.C. Liao, F.C. Hsu, N.H. Tai, M.K. Wu, J. Electrochem. Soc. 152 (2005) A653–A657.
[29] M.V. Reddy, B. Pecquenard, P. Vinatier, A. Levasseur, J. Phys. Chem. B 110 (2006) 4301–4306.
[30] F. Abbattista, M. Vallino, D. Mazza, Mater. Chem. Phys. 15 (1986) 495–503.
[31] W.E. Tenhaeff, E. Rangasamy, Y. Wang, A.P. Sokolov, J. Wolfenstine, J. Sakamoto, N.J. Dudney, ChemElectroChem 1 (2014) 375–378.
[32] M. Stanislowski, E. Wessel, T. Markus, L. Singheiser, W.J. Quadakkers, Solid State Ion. 179 (2008) 2406–2415.
[33] S. Indris, P. Heitjans, R. Uecker, B. Roling, J. Phys. Chem. C 116 (2012) 14243–14247.
[34] N. Janani, S. Ramakumar, L. Dhivya, C. Deviannapoorani, K. Saranya, R. Murugan, Ionics 17 (2011) 575–580.